Coherent propagation and amplification of intense wave beams in a deformed multicore fiber

A. A. Balakin,* A. G. Litvak, and S. A. Skobelev
Institute of Applied Physics of the Russian Academy of Sciences, 603950 Nizhniy Novgorod, Russia

(Received 20 January 2020; accepted 27 July 2020; published 24 August 2020)

The transformation of the out-of-phase distribution of the wave field at a structural deformation of a multicore fiber (MCF), including fiber bending and gain inhomogeneity in different cores, is studied. A nonlinear supermode is found, which is weakly sensitive to deformations of the MCF in the case of high-power radiation. It is shown that nonuniformity of the wave field amplitude in different cores decreases with an increase in the total radiation power. In particular, amplification of the wave beam in the form of the found out-of-phase solution in an active MCF leads to equalization of the wave field amplitudes in all cores at a power exceeding the found critical value even in a strongly deformed MCF. Additionally, approximate expressions of spatiotemporal solitons were found in such MCF, the existence and stability of which is confirmed by direct numerical simulation.

DOI: 10.1103/PhysRevA.102.023527

I. INTRODUCTION

The problem of constructing fully fiber laser systems for generation of high-power laser beams is still relevant today. The interest in replacing high-power solid-state lasers by equivalent fiber laser systems is due to their small sizes, ease of control, reliability, and stability. However, an obvious drawback of fiber systems is the operation with low-power laser beams. This limitation is associated with both a change in the spatial structure of high-power radiation due to the media nonlinearity or the development of filamentation instability and nonlinear absorption in the medium, which leads to fiber damage.

To obtain laser pulses with an extremely high-power level, it is feasible to use an array of independent active optical fibers and then combine laser pulses from many fibers coherently [1,2]. The method of coherent combining of laser beams requires maintaining a constant phase difference between the fibers under conditions of random changes in the beam phase. This idea was demonstrated experimentally for several channels at a rather high peak power [3], and for several tens of channels at a low power [4,5]. A further increase in the number of synchronized optical fibers requires a significant financial and technological effort. The fundamental difficulty is the need to create a feedback system to maintain the phase in each channel.

Multicore fibers (MCFs) with weakly coupled cores draw a considerable interest. The presence of even weak linear coupling between cores can significantly reduce the sensitivity to phase fluctuations of the injected beams within the problems of coherent transport and combining of laser radiation.

Intensive work has been done related to the study of the nonlinear wave dynamics in discrete systems [6–8]. Discrete solitons are found in both conservative systems, within the framework of the discrete nonlinear Schrödinger equation [8–16], and in active systems, within the framework of the discrete Ginzburg-Landau equation [17–20]. The main difference between nonlinear dynamics in discrete media and the continuum case is the possibility of a discrete collapse (localization on the scale of the lattice period) of the initially wide distribution of the wave field even in the one-dimensional case [11,21]. Such a regime was demonstrated experimentally in Ref. [12], and the corresponding critical power $\mathcal{P}_d$ [21] was analytically found, which differed from the critical power of self-focusing in a homogeneous medium $\mathcal{P}_{\rm cr}$. If the power of the injected beam is significantly higher than the critical power, the wave field stratifies into a set of incoherent structures [22].

In the case of smooth wave field distributions, the presence of the intrinsic critical power $\mathcal{P}_d < \mathcal{P}_{\rm cr}$ does not allow coherent propagation of radiation in most of the MCF cores due to the discrete self-focusing process. Nevertheless, the effects of nonlinear pulse propagation, which are usually undesirable in many applications, can be used advantageously for nonlinear summation and pulse compression [22–32], the formation of light bullets using MCF [15,30–36].

Recently, the research focus has shifted to MCF made of a small number of cores, e.g., MCF consisting of a central core and an even number $2N$ of cores located around a ring [24–26,37–39]. For such MCF, stable inhomogeneous stationary nonlinear wave field distributions with a total power being much larger than the critical self-focusing power [29,39] were found. Of greatest interest is the strongly rugged out-of-phase distribution ($\pm$ mode), in which the total radiation power can be many times higher (up to $2N$ times) than the critical self-focusing power in a homogeneous medium.

Along with the beam problem, stable spatiotemporal soliton solutions were found [29]. The existence of these nonlinear solutions made it possible to generalize the well-known methods of compression of laser pulses in a single fiber for MCF, which will make it possible to take a significant step in solving the problem of the formation of high-energy and short-duration laser pulses in fully fiber systems.

*balakin@appl.sci-nnov.ru

A very important question is the kind of transformation of the ± mode upon deformation of the MCF structure, including its bending and gain inhomogeneity in different cores. In this paper, we determine the conditions, under which the inhomogeneity of the amplitude of the out-of-phase distribution remains small. It is shown that the nonuniformity of the wave field amplitude in different cores decreases with an increase in the total radiation power. In particular, wave beam amplification in an active MCF even with a strong difference in the refractive indices of its cores leads to equalization of the wave field amplitudes in the cores at a power exceeding some critical value determined for the parameters of a specific MCF.

Along with the beam problem, the presence of coherent solitonlike optical pulses in MCFs, that can propagate along extended paths without change, is of interest. This is the three-dimensional spatiotemporal solutions that retain their shape due to the balance of diffraction, group velocity dispersion, and nonlinear phase modulations. Similar solutions were found in Refs. [29,32]. In this regard, the question arises as to the existence of such solutions in a strongly deformed MCF.

The paper is structured as follows. In Sec. II, the basic equations are formulated. Section III analyzes the mode stability in the case of small deformations. In Sec. IV, stability analysis of the ± mode with respect to the linear amplification process in MCF is performed for the case of a nonuniform gain across cores. In Sec. V, the out-of-phase distribution is found in the case of strong MCF bending. In Sec. VI, the wave field amplification is analyzed in the active MCF in order to obtain a laser pulse with a total power that is many times higher than the critical self-focusing power in a homogeneous medium. Approximate solutions for spatiotemporal solitons in strongly bent MCFs are presented in Sec. VIII. Section VII contains the results of direct numerical simulation within the framework of a more general model. In conclusion, the main results of the work are formulated.

II. PROBLEM FORMULATION

Let us consider the wave field self-action in a multicore fiber (MCF) made of an even number of cores ($2N$) arranged in a ring. We assume that the fundamental guided modes are oriented in parallel to the z axis of optical single-mode lightguides weakly coupled to each other. Then the propagation of electromagnetic radiation in the MCF can be approximately described as a superposition of modes localized in each core,

$$E(z,x,y,t) \simeq \sum_n \mathcal{E}_n(z)\psi(x-x_n,y-y_n)e^{i\kappa z-i\omega t} + \text{c.c.}, \tag{1}$$

where $\psi(x,y)$ is the structure of the fundamental mode in a core, $\mathcal{E}_n$ is the envelope of the electric field strength in the nth core, which slowly changes along the z axis. The evolution of $\mathcal{E}_n$ during the wave field propagation along the z axis can be affected by the Kerr nonlinearity, amplification in the active medium, and interaction with the neighboring cores arising from weak overlapping of the wave modes directed by them. Assuming that the core coupling is weak and does not perturb the structure of the fundamental mode, we obtain the following equations for the envelope of the electric field $\mathcal{E}_n$ in the nth core:

$$i\frac{\partial \mathcal{E}_n}{\partial z} = \sum_{m=1}^{2N} \chi_{mn}\mathcal{E}_m + \beta_n|\mathcal{E}_n|^2\mathcal{E}_n + i\Gamma_n\mathcal{E}_n. \tag{2}$$

Here, the index n varies from 1 to $2N$, $\chi_{mn} = \chi_{nm}$ determines the coupling strength between the mth and nth cores, and $k_n = \chi_{nn}$, β_n, and Γ_n are the wave number, the nonlinearity coefficient, and the gain in the nth core, respectively.

We assume that all cores are *almost* identical, i.e., the nonlinearity coefficients $\beta_n \equiv \beta$, gain $\Gamma_n = \Gamma + \delta\Gamma_n$, and coupling coefficients $\chi_{nm} = \chi\delta_{m,n\pm1} + k_n\delta_{mn} + \delta\chi_{nm}$ are almost identical for all cores ($|\delta\Gamma_n| \ll \Gamma$ and $|\delta\chi_{nm}| \ll \chi$). The propagation constants $k_n = k + \delta k_n$ in different cores may differ stronger, which corresponds to structural defects (for example, bending). The system of equations (2) is conveniently rewritten in the dimensionless form,

$$i\frac{\partial u_n}{\partial z} = |u_n|^2u_n + u_{n+1} + u_{n-1} + \zeta_{nm}u_m + (h_n + i\gamma_n)u_n. \tag{3}$$

Here, the evolutionary coordinate z is normalized to the coupling coefficient χ, $u_n = e^{-ikz}\mathcal{E}_n/\sqrt{\beta}$ is the complex amplitude of the wave field envelope in the nth core, $\zeta_{nm} = \delta\chi_{nm}/\chi \ll 1$, $h_n = \delta k_n/\chi$, and $\gamma_n = \Gamma_n/\chi$. The effect of temporal dispersion will be considered in Sec. VIII. During evolution, the system of equations (3) with $\gamma_n = 0$ preserves the total power of the wave beam,

$$P = \sum_{n=1}^{2N} |u_n|^2 = \text{const}. \tag{4}$$

Equation (3) was obtained in the framework of the approximation of the single-mode wave field propagation in each of the core. It is violated when the radiation power in any core $\mathcal{P}_n = |\mathcal{E}_n|^2 \iint \psi^2 dxdy$ is close to the critical self-focusing power $\mathcal{P}_{\text{cr}}$ in homogeneous media.

In the case of ideal cores ($\zeta_{nm} = h_n = 0$) without amplification ($\gamma_n = 0$), stable exact solutions for intense wave beams in MCF were found in Ref. [39], which allowed coherent transport of laser beams over long distances. The total beam power in this case can exceed significantly the critical self-focusing power in homogeneous media. Of greatest interest is the solution in the form of "± mode":

$$u_n = (-1)^n f_N, \tag{5}$$

in which the total power can exceed the critical power of self-focusing in homogeneous media significantly (by up to $2N$ times). Moreover, this solution is stable and exists at all wave field amplitudes.

Indeed, let us study solution (5) with respect to filamentation instability. For $N \geqslant 2$ and a wave field with perturbations having the form ($\kappa_s = \pi s/N$),

$$u_n = [(-1)^n f_N + \delta_s e^{i\lambda_s z + i\kappa_s n}]e^{i(2-f_N^2)z},$$

we get real eigenvalues assuming $|\delta_s| \ll f_m$ and $\kappa_s \neq \pi$,

$$\lambda_s^2 = 4[1+\cos\kappa_s]\left[1+\cos\kappa_s + f_N^2\right] > 0. \tag{6}$$

Below in this paper, we find similar solutions and analyze their stability with respect to the deformation of the MCF structure ($\zeta_{nm}, h_n \neq 0$) and gain ($\gamma_n \neq 0$).

III. WEAK DEFORMATIONS ($\zeta_{nm}, h_n \ll 1, \gamma_n = 0$)

A deformation of the MCF structure leads, first of all, to differences in the refractive indices in cores. A typical example of a linear change in the refractive indices is

$$h_n = D \sin \frac{\pi n}{N}, \quad \zeta_{nm} = 0, \tag{7}$$

resulting from bending of optical fibers. Here, D is the perturbation amplitude. This is also a leading term of the Fourier expansion of an arbitrary perturbation of the refractive index.

The appearance of large-scale fluctuations means, as a rule, that all linear eigenmodes of the MCF are excited, which makes the problem difficult for analytical consideration. However, if the value of D is not too large, the perturbations of the mode $(-1)^n$ remain small. In this case, an approximate solution of Eq. (3) for $N \geqslant 2$ can be sought for in the form,

$$u_n = f_N e^{i(2-f_N^2)z}[(-1)^n + \delta_n], \quad |\delta_n| \ll 1. \tag{8}$$

Substituting (8) into Eq. (3), we find the following for the stationary solution in the first order of smallness in $\delta_n \propto \xi_n = h_n + \sum_m (-1)^{m-n}\zeta_{nm}$:

$$\begin{aligned} \left(f_N^2 - 2\right)\delta_n &\approx \xi_n(-1)^n + \delta_{n+1} + \delta_{n-1} + 3f_N^2\delta_n, \\ \Rightarrow \delta_n &\approx \sum_m \sum_{k\neq N} \frac{\xi_m(-1)^m e^{i\varkappa_k(n-m)}}{2N\left(4\cos^2\frac{\varkappa_k}{2} + 2f_N^2\right)}, \end{aligned} \tag{9}$$

where $\varkappa_k = k\pi/N$. Here, we have taken into account that for real ξ_n we can assume, without loss of generality, that f_N and δ_n are also real. For perturbations of the form of (7), the solution is simplified:

$$\delta_n \approx -\frac{D}{4\sin^2\frac{\pi}{2N} + 2f_N^2}(-1)^n \sin\frac{\pi n}{N}. \tag{10}$$

These formulas show that the perturbations remain small ($|\delta_n| \ll f_N$), as far as the perturbation of the refractive index is small: either $|\xi_n| \ll 4\sin^2\frac{\pi}{2N} \leqslant 2$, or $|\xi_n| \ll 2f_N^2 = P/N$. Note that the power fraction in the perturbation is a quantity of the following order of smallness due to the orthogonality of any perturbations and the variety of solutions $(-1)^n$:

$$\delta P = \sum_n |u_n|^2 - 2Nf_N^2 = \sum_n |\delta_n|^2. \tag{11}$$

The similarity of cores results in equal weights of 1 when calculating the orthogonality of the distributions. In the particular case of perturbations (7), the expression for the power fraction in the perturbations becomes simpler:

$$\frac{\delta P}{P} \equiv 1 - \eta_\pm = \frac{D^2}{4\left(4\sin^2\frac{\pi}{2N} + P/N\right)^2}. \tag{12}$$

Next, we turn to the results of numerical simulation of Eq. (3) under perturbations having the form of Eq. (7). The relative phase difference of the field in neighboring cores was preserved in numerical simulations and amounted to π. Figures 1(a) and 1(b) shows two surfaces of different colors, which represent the dependence of the power fraction $\eta_\pm = 1 - \delta P/P$ in the $\pm$ mode on the amplitude perturbations of D of the refractive index h_n and of the total power P for different numbers of cores in a passive MCF: six cores ($N = 3$) and 20 cores ($N = 10$) [Figs. 1(a) and 1(b), respectively].

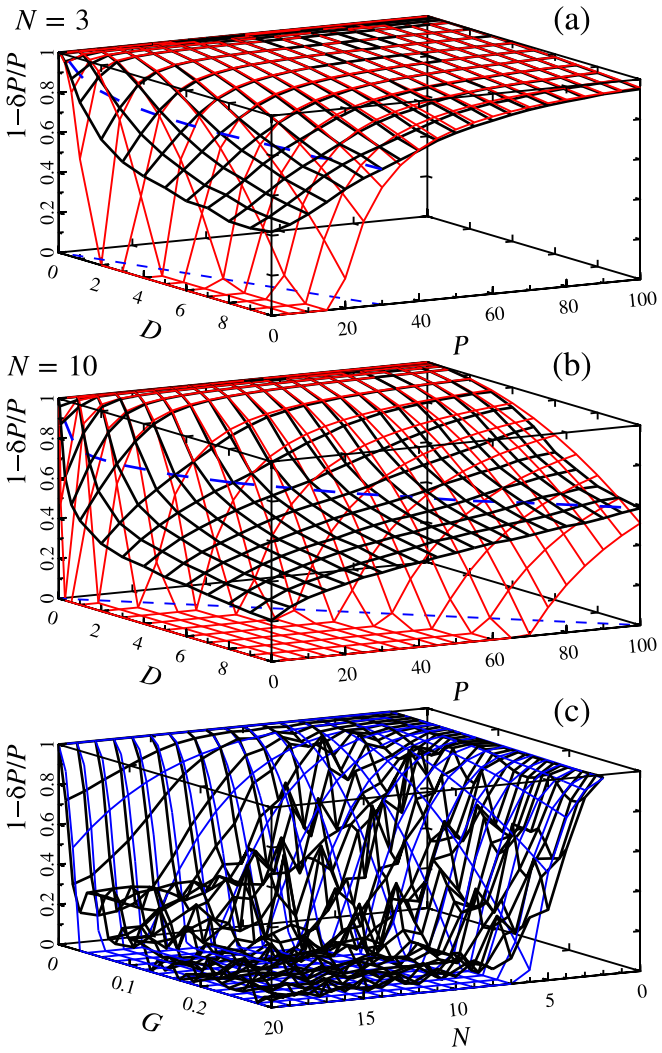

FIG. 1. (a) and (b) Dependence of the power fraction $\eta_\pm$ in the $\pm$ mode on the amplitude of deformations D and on the total power P for different number of cores $2N$ in a passive MCF ($\gamma_n = 0$). Black lines are the results of numerical simulations of Eq. (3). Red (gray) lines correspond to approximation (12). The blue dash line shows boundary (13). (c) Dependence of the power fraction $\eta_\pm$ in the $\pm$ mode in the active MCF on the number of cores $2N$ and on the amplitude of the gain perturbations G at $D = 0$ and $\gamma = 0.01$. Blue (gray) lines correspond to estimate (19).

Here, the black lines are based on the results of numerical simulations of Eq. (3), and the red (gray) lines correspond to the found approximation (12). It can be seen that an increase in the amplitude D leads to an increase in the fraction of the perturbation power $\delta P/P$ and, thereby, to a decrease in the maximum transported radiation power in the out-of-phase mode via MCF. The power fraction $\eta_\pm$ in the linear case $P \ll 4N\sin^2\frac{\pi}{2N} \leqslant 4$ is close to unity only when the perturbation amplitude D lies in the narrow range of $D \ll D^* \equiv 4\sin^2\frac{\pi}{2N}$. Moreover, this range narrows rapidly with an increase in the number of cores [see Figs. 1(a) and 1(b)]. On the contrary, most of the power is contained in the $\pm$ mode when powerful radiation is transported:

$$P \gg P_{\text{th}} \equiv DN. \tag{13}$$

For example, in the case of six cores ($N = 3$), the threshold power at $D = 5$ is $P_{\rm th} = 15$, and for 20 cores ($N = 10$) we get $P_{\rm th} = 50$. Thus, in general, the found approximation (12) is in good agreement with the results of numerical simulation of Eq. (3) [see Figs. 1(a) and 1(b)].

IV. ACTIVE MCF ($\zeta_{nm} = h_n = 0$, $\gamma_n \ll 1$)

Let us analyze stability of the $\pm$ mode with respect to the process of weakly inhomogeneous linear amplification in active MCF. An approximate solution of Eq. (3) in the case of $|\delta_n| \ll f_N$ will be sought in the form,

$$u_n = [(-1)^n + \delta_n e^{i\varkappa_s n}] f_N e^{\gamma z + 2iz - i\exp(2\gamma z)/2\gamma}. \quad (14)$$

Substituting (14) into Eq. (3), we find

$$i\frac{\partial \delta_n}{\partial z} - 2\delta_n = f_N^2(\delta_n + \delta_n^*) + 2\delta_n \cos\varkappa_s + i\sum \delta\gamma_m (-1)^m e^{-i\varkappa_n m}, \quad (15)$$

where $\gamma = \sum \gamma_n/2N$ and $\delta\gamma_n = \gamma_n - \gamma$. We first analyze the stability of the out-of-phase mode in the case of the same gain in all cores ($\delta\gamma_n = 0$). Obviously, the field growth is small on the scale of the coupling length (~ 1) in the case of $\gamma \ll 1$. So, one can find the local dispersion relation for $\delta_n \propto e^{i\lambda z}$,

$$\lambda^2(z) \approx 8\cos^2\left(\frac{\varkappa_n}{2}\right)\left[2\cos^2\left(\frac{\varkappa_n}{2}\right) + f_N^2(z)\right] \geqslant 0,$$

from which it follows that the perturbation amplitudes grow no faster than the $\pm$ mode.

Next, we consider the field amplification in MCF in the case of a spread of the gain $\delta\gamma_n \neq 0$ over cores. The forced solution of Eq. (15) has the form,

$$\delta_n \approx -\frac{if_N}{2N}\sum_m \sum_{k\neq N} \frac{\delta\gamma_m (-1)^m e^{i\varkappa_k (n-m)}}{4\cos^2\frac{\varkappa_k}{2}}. \quad (16)$$

For example, let us consider the most dangerous case of $\delta\gamma_n = G\sin\frac{\pi n}{N}$. As a result, we obtain an approximation of the amplitudes of the field perturbations in the active MCF,

$$\delta_n \approx -\frac{iG(-1)^n \sin\frac{\pi n}{N}}{4\sin^2\frac{\pi}{2N}}. \quad (17)$$

It follows that the perturbations remain small ($|\delta_n| \ll f_N$), in so far as the gain perturbation is small,

$$G \ll 4\sin^2\frac{\pi}{2N}. \quad (18)$$

The expression for the power fraction in perturbations takes the form similar to (12),

$$\frac{\delta P}{P} \equiv 1 - \eta_\pm = \frac{G^2}{64\sin^4\frac{\pi}{2N}}. \quad (19)$$

Thus, the effects of gain inhomogeneity will be noticeable only for a large number of cores:

$$N \gg N_{\rm lim} \equiv \pi/\sqrt{G}, \quad G \ll \gamma \ll 1. \quad (20)$$

Next, we turn to the results of the numerical simulation of Eq. (3). Figure 1(c) shows the dependence of the power fraction $\eta_\pm$ in the $\pm$ mode in the active MCF as a function of the number of cores $2N$ and the amplitude of the gain perturbation G. The calculation was performed for the average gain $\gamma = 0.01$ and $D = 0$. Black lines correspond to the results of the numerical simulation of the initial equation, Eq. (3). Blue dash lines correspond to the estimate (19). The gain inhomogeneity across the cores affects weakly the radiation amplification in the MCF (most of the radiation power is contained in the $\pm$ mode) in the case of $N \ll N_{\rm lim}$ [Fig. 1(c)]. For example, a significant power fraction ($\eta_\pm \approx 0.9$) can be produced in an MCF of 40 cores ($N = 20 \lesssim N_{\rm lim}$) in the case of a small gain spread, $G = 0.01$. However, it is necessary to use MCF with a smaller number of cores with an increase in the coefficient G. For example, the power fraction $\eta_\pm \approx 0.8$ at $G = 0.3$ is realized only in the case of 10 cores ($N = 5 \lesssim N_{\rm lim}$). The significant drop in the power fraction in the $\pm$ mode takes place for $N > N_{\rm lim}$ [see Fig. 1(c)]. Note that the strong ruggedness of the power fraction $\eta_\pm$ on G and N (black line surface) is associated with strong radiation scattering from the $\pm$ mode to other eigenmodes and further amplification of the scattered radiation. Thus, estimate (19) for the power fraction in the $\pm$ mode and the limiting number of MCF cores (20) are in good agreement with the results of the numerical simulation [see Fig. 1(c)].

V. STRONG MCF BENDING ($\zeta_{nm} = \gamma_n = 0$)

Section III shows that a small MCF deformation changes the $\pm$ mode (5) weakly during radiation transportation ($\eta_\pm \approx 1$) in the case of weak bending of the MCF ($D \ll D^*$) and in the case of strong radiation ($P \gg P_{\rm th}$). Otherwise, the spatial distribution of the out-of-phase wave distribution in the deformed MCF differs significantly from the ideal case [mode $u_n^{D=0} \propto (-1)^n$]. This means that the distribution $u_n^{D=0}$ is not a stationary solution and, accordingly, will be split up into eigenmodes of an arbitrarily strongly deformed MCF. Obviously, the power fraction in the distribution of $u_n^{D=0}$ will decrease with increasing difference between this distribution and the out-of-phase stationary solution in curved MCF.

In this section, we find stationary solutions of the deformed MCF. The complexity of finding analytical solutions increases quite rapidly with an increase in the number of cores. Therefore, we restrict ourselves to the case of six cores ($N = 3$) in the analytical calculations presented in the paper, when perturbations of the form (7) in out-of-phase solutions of Eq. (3) generate a small number of eigenmodes: $(-1)^n$, $\cos\frac{\pi n}{3}$, and $\sin\frac{2\pi n}{3}$. Then, the use of the total power conservation law (4) allows us to search for the solution in the form,

$$u_n = C\sqrt{\frac{P}{6}}(-1)^n e^{i\sigma} + B\sqrt{\frac{P}{3}}e^{i\sigma + i\phi}\sin\frac{2\pi n}{3} + A\sqrt{\frac{P}{3}}e^{i\sigma + i\theta}\cos\frac{\pi n}{3}, \quad (21)$$

where $C^2 = 1 - A^2 - B^2$ is the power fraction in the mode $(-1)^n$, A^2 and B^2 are the power fractions in the $\sin\frac{2\pi n}{3}$ and $\cos\frac{\pi n}{3}$ modes, respectively, and ϕ and θ are relative phase differences. Substituting field distribution (21) to Eq. (3), we

obtain a system of Hamiltonian equations for changing the parameters of the wave field $\{A^2, B^2, \phi, \theta\}$,

$$\frac{d\theta}{dz} = -\frac{\partial H}{\partial A^2}, \quad \frac{d\phi}{dz} = \frac{\partial H}{\partial B^2}, \tag{22a}$$

$$\frac{dA^2}{dz} = \frac{\partial H}{\partial \theta}, \quad \frac{dB^2}{dz} = \frac{\partial H}{\partial \phi}, \tag{22b}$$

with the Hamiltonian,

$$\begin{aligned}\frac{H}{P} = &-\frac{AB^2C}{3\sqrt{2}}\cos(2\phi-\theta) + \frac{A^2B^2}{12}\cos(2\phi-2\theta)\\ &+ABD\cos(\phi-\theta) - \sqrt{2}CBD\cos\phi\\ &+\frac{C^2}{6}(A^2\cos 2\theta + B^2\cos 2\phi)P\\ &+(A^2-2B^2)\frac{APC}{3\sqrt{2}}\cos\theta + B^2 + 3A^2\\ &-\frac{P}{8}(B^4+A^4) + \frac{P}{6}(A^2 - 2A^2B^2 + B^2).\end{aligned} \tag{23}$$

Note that the equation for the evolution of the common phase σ is split off from the dynamics of other wave beam parameters due to the conservation of the total power P.

Resulting equations (22) describe the dynamics of the wave beam parameters in the four-dimensional phase space, and the dynamics themselves can be quite complex. Fortunately, we are only interested in stable stationary solutions, which are determined by the equilibrium states of Eq. (22).

Note that Eq. (22) are written not for canonically conjugate variables. For this system, the canonically conjugate coordinates are $\{\theta, A^2\}$ and $\{\phi, B^2\}$. However, we introduced the quantities A and B specially, because they allowed the whole variety of equilibrium states $\theta_k = \pi k$, $\phi_l = \pi l$ of Eq. (22) to be reduced to the only case of $\theta = \phi = 0$. At this, the sign of the quantities A and B will determine the indices $k = 0, 1$ and $l = 0, 1$. At the same time, we avoided singularities at $A = 0$ and $B = 0$, which are present when canonically conjugate variables are used.

So, in order to find stationary solutions, it is sufficient to find the minima and maxima of Hamiltonian (23) for $\theta = \phi = 0$,

$$\begin{aligned}H_0 \equiv &\frac{H_{\theta=0,\phi=0}}{P}\\ &= ABD + B^2 + 3A^2\\ &\quad -\sqrt{1-A^2-B^2}\frac{3AB^2P - A^3P + 6BD}{3\sqrt{2}}\\ &\quad +\frac{(B^2+A^2)P}{3} - \frac{7(B^2+A^2)^2P}{24},\end{aligned} \tag{24}$$

and determine their stability. The search for equilibrium states is a rather difficult task from the analytical point of view, since it is necessary to solve the transcendental equation. The form of the Hamiltonian H_0 and the numerically found equilibrium states for various values of P and D are shown in Fig. 2.

There is only one equilibrium state (Fig. 2), which is close to the ± mode ($A, B \approx 0$), for a small bending of $D = 0.1 \ll D^* = 3$ and for a total power of $P = 1 \gg P_{\text{th}} = DN = 0.3$. This equilibrium state is marked with the symbol ± in the figure. With increasing power, the following equilibrium states appear (see the top row in Fig. 2). The asterisks indicate the position of the equilibrium states of Eq. (22). For example, there are four equilibrium states for $P = 10$, and there are already six equilibrium states for $P = 100$. It can be seen that the position of the equilibrium state corresponding to the out-of-phase solution shifts weakly from the point ($A \approx B \approx 0$) in the large range of the total power P (see Fig. 2). This means that solution (21) corresponding to the equilibrium states ($A \approx B \approx 0, C \approx 1$) is slightly different from the distribution of the solution $(-1)^n$ of nondeformed MCF, i.e., the power fraction in the ± mode is close to unity, which agrees with the results of numerical simulation (see Fig. 1).

The insets in Fig. 2 show the typical spatial distribution of the wave field in the MCF corresponding to different equilibrium states. Note that injection of a wave beam with a spatial distribution corresponding to the equilibrium states at the MCF input yields no beating of the wave field during its propagation.

It is possible to find an approximation of equilibrium states only for small perturbations of the refractive index $D \ll D^*$ or for high powers $P \gg P_{\text{th}}$. Of greatest interest is the out-of-phase solution:

$$B_\pm \approx \frac{3\sqrt{2}D}{2P+6} + O(D^3), \tag{25a}$$

$$A_\pm \approx \frac{9(P-6)D^2}{4\sqrt{2}(P+3)^2(P+9)} \ll B_\pm. \tag{25b}$$

It can be seen that strong bending of MCF leads first of all to an increase in the coefficient B [according to (10)], and only in the second order of smallness, to an increase in the coefficient A (see Fig. 2). This, together with the orthogonality of the eigenmodes $\sin\frac{2\pi n}{3}$ and $\cos\frac{\pi n}{3}$, makes the range of applicability of Eq. (10) rather wide.

It is also possible to find approximations of the remaining six equilibrium states at high powers $P \gg P_{\text{th}}$ (Fig. 2):

$$A_1 \approx \sqrt{\frac{2}{3}}\left(1 + \frac{2}{P} - \frac{8}{P^2}\right), \quad B_1 \approx \frac{2\sqrt{6}D}{P^2},$$

$$A_{2,3} \approx \sqrt{\frac{2}{3}}\left(\frac{1}{2} - \frac{2}{P} - \frac{5 \pm 2\sqrt{3}D}{P^2}\right), \quad B_{2,3} \approx \frac{\pm 1}{\sqrt{2}} \mp \frac{3\sqrt{2}}{P^2},$$

$$A_4 \approx -\frac{2\sqrt{2}}{3}\left(1 - \frac{1}{P}\right), \quad B_4 \approx \frac{3D}{\sqrt{2}P},$$

$$A_{5,6} \approx \frac{\sqrt{2}}{3}\left(1 - \frac{5 \pm \frac{3}{2}\sqrt{3}D}{P}\right), \quad B_5 \approx \pm\sqrt{\frac{2}{3}}\left(1 + \frac{1}{P}\right).$$

These approximations show that equilibrium states 1, 2, and 3 have a weaker dependence on the deformation amplitude ($\propto D/P^2$) than equilibrium states 4, 5, and 6 ($\propto D/P$). In other words, only three (4, 5, and 6) of the six equilibrium states are sensitive to bending. This is due to the symmetry of equilibrium states 1, 2, and 3, which suppresses the effect of curvature. Formal stability analysis of these solutions,

$$\left(\frac{\partial^2 H}{\partial\theta\partial\phi}\right)^2 < 4\frac{\partial^2 H}{\partial\theta^2}\frac{\partial^2 H}{\partial\phi^2}, \quad \frac{\partial^2 H}{\partial\theta^2}\frac{\partial^2 H}{\partial A^2} \geqslant 0, \tag{27}$$

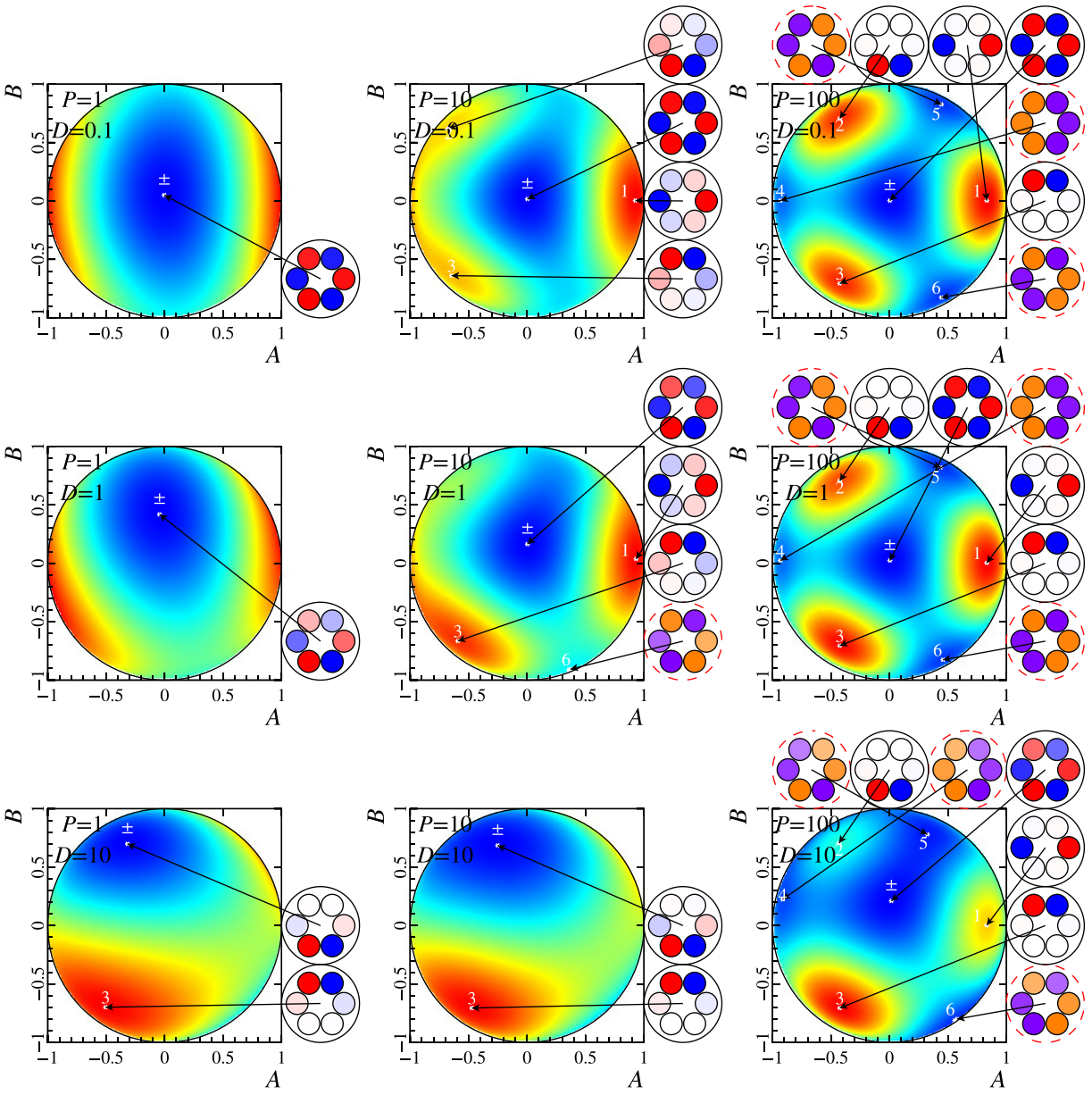

FIG. 2. Form of the Hamiltonian (24) for various P and D. Asterisks indicate the position of the equilibrium states of Eq. (22). Insets show the field distribution at these equilibrium states. Unstable field distributions are marked with dashed circles.

yields the stability of solutions 1, 2, and 3. Solutions 4, 5, and 6 lose stability at $D \to 0$. The most interesting out-of-phase mode (25) is always stable, since it has the largest propagation constant. Therefore, its decay into other modes is energetically unprofitable [29].

Further analysis will be limited to only the $\pm$ equilibrium state, which is of the greatest practical interest. Figure 2 shows that the position of this point shifts quite strongly in the plane (A, B) with the increasing coefficient D at a small value of the total power $P \ll P_{\text{th}}$. Figure 3(a) shows the dependencies of the parameters A, B, C of the out-of-phase solution (21) depending on the power P and the bending coefficient D.

Unlike weak bending ($D \ll D^*$ or $P \gg P_{\text{th}}$), the parameters A and B of the solution of Eq. (21) change at approximately the same rate as an increase in the bending coefficient D. As a result, solution (21) differs significantly from the distribution of the $\pm$ mode (5) in a nondeformed MCF. This is confirmed by the spatial distribution of the wave field corresponding to the $\pm$ equilibrium state shown in the insets of Fig. 2 for ($P = 1 \ll P_{\text{th}} = 3$, $D = 1$), ($P = 1 \ll P_{\text{th}} = 30$, $D = 10$), and ($P = 10 \ll P_{\text{th}} = 100$, $D = 10$). It follows from the given inserts that the wave field is predominantly localized out-of-phase only in two neighboring MCF cores, where the amplitude of the perturbation of the refractive index is minimal ($h_n \approx -D$). In this case, the fraction $\eta_{\pm}$ decreases [Fig. 3(c)], but not as much as the approximation (12) (red lines).

In the case of high-power radiation ($P \gg P_{\text{th}}$), the position of the equilibrium state $\pm$ shifts again towards $A, B \approx 0$ (Fig. 2). For example, consider the following cases: (i) $P = 10 \gg P_{\text{th}} = 3$, $D = 1$, (ii) $P = 100 \gg P_{\text{th}} = 3$, $D = 1$, and (iii) $P = 100 \gg P_{\text{th}} = 30$, $D = 10$. This corresponds to the

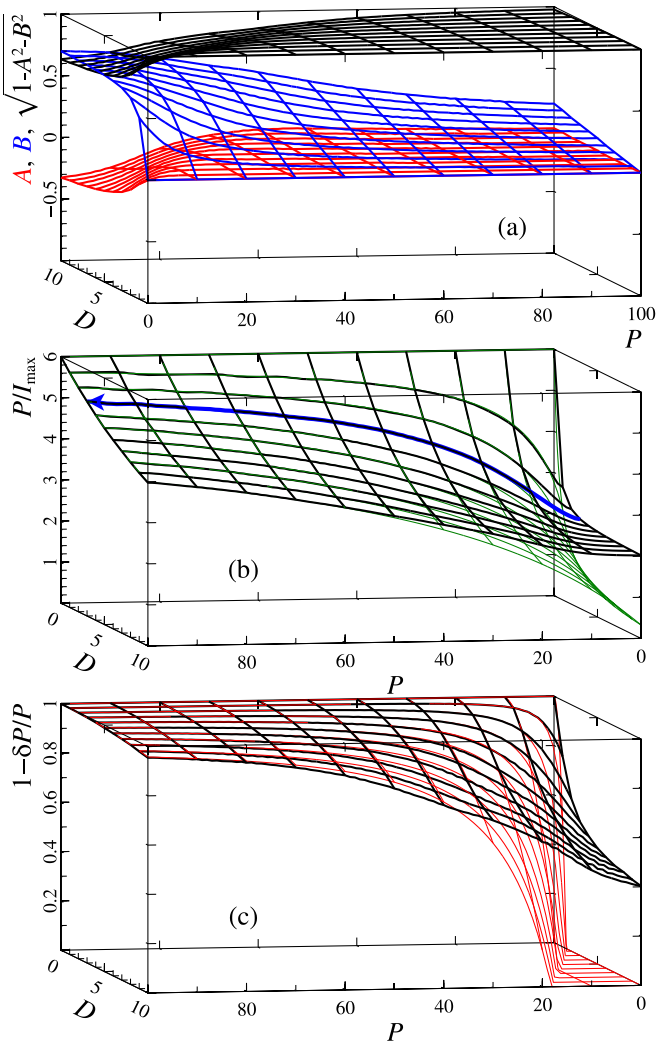

FIG. 3. (a) Form of the out-of-phase solution depending on the parameters P and D. (b) Dependence of the maximum intensity $P/\max_n |u_n|^2$ (black) on this solution and its approximation (29) (green). The blue curve with an arrow shows the change in the maximum intensity with a smooth increase in power. (c) The dependence of the power fraction $\eta_\pm = 1 - \delta P/P$ in the $\pm$ mode (black) on the out-of-phase solution and its approximation (12) (red).

almost uniform wave field distribution in all MCF cores ($C \approx 1$), and the power fraction becomes $\eta_\pm \approx 1$. This conclusion is in good agreement with Fig. 3. Therefore, the nonlinearity of the medium "straightens" the out-of-phase mode of the deformed MCF to the form of $(-1)^n$ in the case of high-power radiation $P \gg P_{\text{th}}$.

As noted in the Introduction, the interest in MCF is related to the ability to split the total high-power P into channels with powers below any undesirable nonlinear effects that can lead to fiber damage. However, as shown above, strong deformations of the six-core MCF lead to strong localization of radiation in only two cores. This means that the maximum intensity in the cores at a fixed total power P will be much higher than in the case of the uniformly distributed wave field over all the cores (5). At this, the power in a separate core is determined by only the dimensionless intensity $I_n = |u_n|^2$. In dimensional units, this is $\mathcal{P}_n = |\mathcal{E}_n|^2 \iint \psi^2 dxdy$.

Knowing equilibrium states (21) allows us to find the maximum value of the field intensity for a fixed power: $I_{\max} = \max_n |u_n|^2$. The maximum intensity $I_{\max}$ is the important characteristic that allows one to estimate the maximum transported power before any damage to MCF occurs. Indeed, no more power than the critical self-focusing power $\mathcal{P}_{\text{cr}}$ can be placed in each core. Then, the maximal total power can be estimated as

$$\mathcal{P} \leqslant \frac{P}{I_{\max}} \mathcal{P}_{\text{cr}}. \tag{28}$$

Obviously, the minimum $I_{\max}$ is reached at solution (25), which is close to the $\pm$ mode, where the field intensity is distributed uniformly over all the kernels $I_n = P/2N$. Nevertheless, an increase in the bending amplitude D leads to a skew of the wave distribution and a decrease in the maximum transported power. Moreover, the maximum intensity depends mainly on the ratio D/P and is approximated well by the formula,

$$\frac{6}{P} I_{\max} \approx 1 + \frac{3\sqrt{3}D}{P+3}, \quad D \ll P + 3. \tag{29}$$

At its maximum, the value of $I_{\max}$ reaches 3, which corresponds to a field concentrated only in two of the six cores. Figure 3(b) shows the dependence of the maximum intensity $P/I_{\max}$ on the out-of-phase solution (black surface) and its approximation (29) (green surface) versus the bending coefficient D and the total power P. Comparison of the exact solution and the approximation shows good agreement up to $I_{\max} \leqslant 2$.

Let us discuss the case of MCF with a large number of cores ($N > 3$). The formally presented procedure for obtaining stationary solutions is easily generalized to the case of arbitrary N. However, the search for analytical solutions becomes difficult with an increase in the number of cores, since perturbations of the form of (7) generate a large number of linear eigenmodes in the out-of-phase solution even for odd $N = 5, 7, \ldots$. Therefore, we do not give similar expressions of the Hamiltonian and asymptotic solutions for $N > 3$ due to their excessive cumbersomeness. In what follows, we restrict our consideration to the solution describing the skew of the out-of-phase solution due to the deformation of the MCF.

Figures 4(a), 4(c), and 4(e) show the dependence of the power fraction in the distribution of $(-1)^n$ in a deformed MCF for a different number of cores: 10 ($N = 5$), 14 ($N = 7$), and 30 ($N = 15$). The black surface is plotted on the basis of the found analytical out-of-phase solutions. The red (gray) surface corresponds to the found approximation, Eq. (12). It can be seen that the approximation found is in good agreement for powers $P \geqslant P_{\text{th}} = DN$.

It is possible to generalize analytically approximation (29) of the maximum intensity $I_{\max}$ to the case of a large number of cores,

$$2N \frac{I_{\max}}{P} \approx 1 + \frac{2D \cos\frac{\pi}{2N}}{4\sin^2\left(\frac{\pi}{2N}\right) + \frac{P}{N}}. \tag{30}$$

Figures 4(b), 4(d), and 4(f) show the dependence of the maximum intensity $P/I_{\max}$ on P and D for a different number of cores. The black surface is plotted on the basis of the exact solution corresponding to the $\pm$ equilibrium state. The green

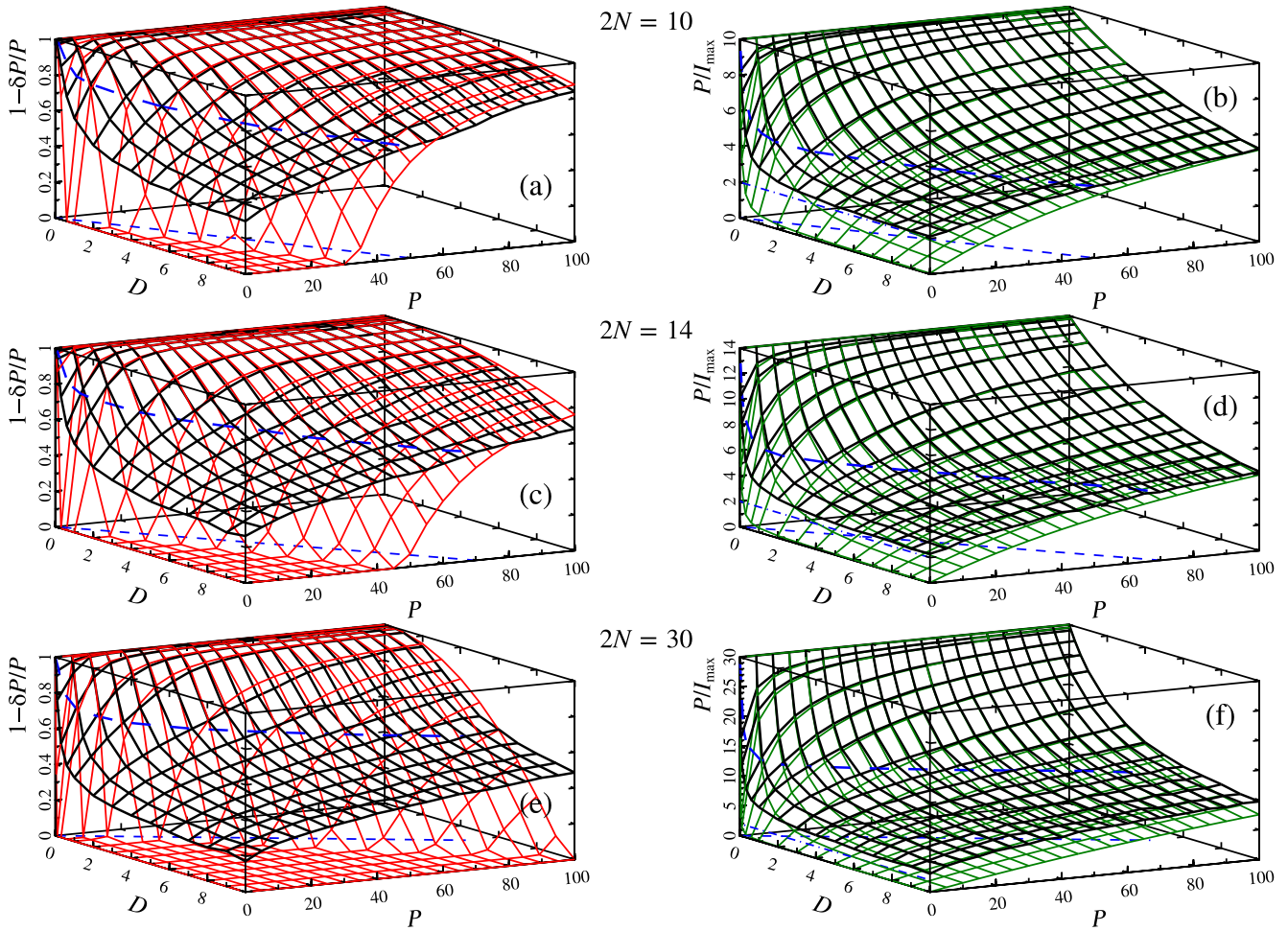

FIG. 4. Dependencies of the power fraction in the ± mode (a), (c), and (e) and the maximum intensity $P/I_{\max}$ (b), (d), and (f) on D and P for different number of cores: 10 ($N = 5$), 14 ($N = 7$), and 30 ($N = 15$). Black surfaces are plotted on the basis of the found out-of-phase solutions. Red and green (gray) surfaces correspond to the approximations (12) and (30), respectively. Blue dash lines shows the boundary (13). Dash-dotted lines in (b), (d), and (f) show the level $P/I_{\max} = 2$.

surface corresponds to approximation (30). One can see a good agreement between them. When the MCF is strongly bent ($D \gg D^*$, $P \ll P_{\text{th}}$), the field is localized only in a small number of cores, as in the case of the six-core MCF ($N = 3$). Therefore, the maximum power that can be transported through MCF, taking into account Eq. (28), is $\mathcal{P}_{\max} \leqslant 2\mathcal{P}_{\text{cr}}$. In the case of high-power radiation $P \gg P_{\text{th}}$, the media nonlinearity weakens the influence of the MCF deformation on the wave field dynamics, and the wave beam tends to a uniform distribution over the cores and the maximum power becomes

$$\mathcal{P} \lesssim \frac{2N}{1 + 2P_{\text{th}}/P} P_{\text{cr}} \leqslant 2N\mathcal{P}_{\text{cr}}. \tag{31}$$

VI. AMPLIFICATION IN A STRONGLY BENT MCF

Let us consider the wave field amplification in an active MCF in order to obtain a laser pulse with a total power that is many times greater than the critical self-focusing power in homogeneous media. Obviously, the MCF deformation ($D \neq 0$) and the gain spread across the cores ($G \neq 0$) can significantly limit maximum achievable power (31). The negative effects associated with the gain inhomogeneity can be weakened significantly if the number of cores in the MCF satisfies the condition (20).

In the case of weak bending of MCF ($D \ll D^* = 4\sin^2\frac{\pi}{2N} \leqslant 2$), the out-of-phase solution is close to the ± mode $u_n \propto (-1)^n$, and it is possible to ensure coherent amplification in all cores for $\gamma \ll 1$. The difference between the out-of-phase solution and the ± mode is determined by the value δ_n in accordance with Eq. (10). However, with an increase in the number of cores $2N$, its applicability threshold decreases rather quickly and, for example, for 30 cores ($N = 15$) it is only $D^* = 0.04$. In the case of strong bending, the out-of-phase solution is skewed and the wave field distribution is strongly inhomogeneous, and only a small part of the cores is involved in radiation transport (see Fig. 4). Accordingly, injection of a wave beam with the distribution $u_n \propto (-1)^n$ is undesirable, since it is far from a stationary solution.

Therefore, an initial distribution close to the desired out-of-phase solution should be used. It is easy to find it if we neglect the nonlinearity of the medium in the case of a small initial power $P \ll P_{\text{th}}$. Then, the problem becomes linear and

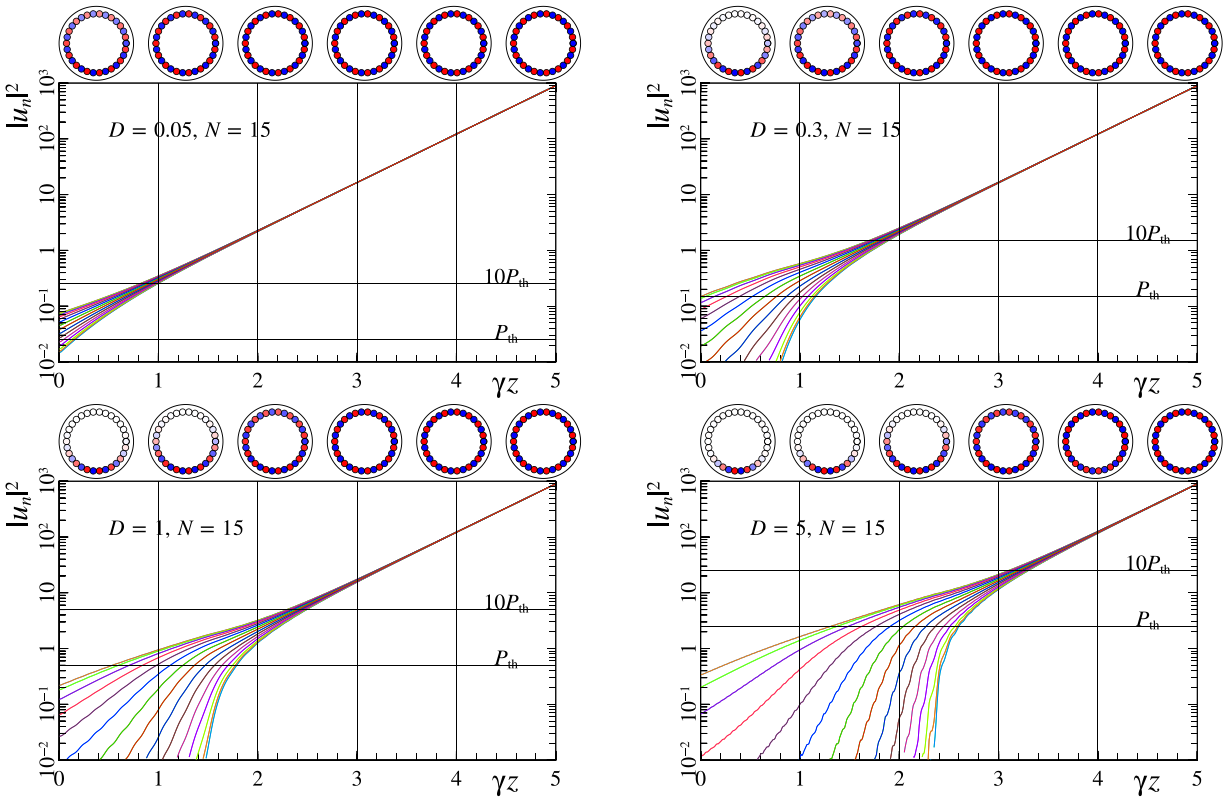

FIG. 5. Dependence of the wave field intensity $|u_n|^2$ in 30-core MCF ($N = 15$) on the evolutionary coordinate z for $D = 4$ (a), $D = 1$ (b), and various γ. The vertical lines show the position of the field distributions in the cores. The horizontal dotted lines denote the level, when the distribution becomes close to the $\pm$ mode.

is reduced to finding the eigenvalues λ and the eigenvectors e_n,

$$A_{nm}e_n^{(k)} = \lambda^{(k)}e_n^{(k)}, \quad \sum e_n^2 = P, \tag{32a}$$

$$\det(A_{nm} - \lambda^{(k)}\delta_{nm}) = 0, \tag{32b}$$

where $A_{n,m} = \delta h_n \delta_{n,m} + \delta_{n,m-1} + \delta_{n,m+1}$. The out-of-phase solution will be the eigenvector corresponding to the minimal (most negative) eigenvalue.

To clarify the process of wave field amplification in a deformed MCF, we consider the six-core MCF, for which analytical relations can be found easily. In Fig. 3(b), the blue curve with the arrow shows the change in the maximum intensity with a smooth increase in the total power. The field is concentrated in several cores for small total powers (Fig. 5), and the intensity is distributed almost uniformly over all the cores for large powers $P \gg P_{\text{th}} = DN$. Consequently, knowledge of the equilibrium states allows one to predict the nonlinear dynamics of the wave field in the active MCF, when the wave power slowly increases at $\gamma \ll 1$ due to the gain being small on the scale of the coupling length. As the wave beam power increases exponentially, an adiabatic rearrangement of the out-of-phase mode is expected.

Numerical simulations of Eq. (3) in an active MCF of 30 cores ($N = 15$) with a gain of $\gamma = 10^{-2}$ and $G = 10^{-3}$ confirm this conclusion clearly. For a given value of the coefficient G, the gain nonuniformity over the cores should not affect the adiabatic rearrangement of the out-of-phase mode, since $N_{\text{lim}} = 100 \gg 15$. Figure 5 shows the evolution of the field intensity in the cores for different coefficients D: $D = 0.05 \simeq D^*$, $D = 0.3$, $D = 1$, $D = 5$. The insets show the typical wave field distributions in different MCF cross sections.

The case of $D = 0.05$ corresponds to weak bending of the MCF. The wave field at the input is distributed quasiuniformly over the cores (Fig. 5). In this case, the initial spread in the field amplitudes is well determined by Eq. (10). At a power of $P = 10P_{\text{th}}$, the intensities in different cores are equalized.

The initial distribution of the wave field becomes more and more anisotropic as the coefficient D increases. Despite this, field intensities become equalized in all the cores again at $P \simeq 10P_{\text{th}} \gg P_{\text{th}}$. In this case, the value $P_{\text{th}} = ND$ grows with an increase in the bending coefficient D and, thus, the transition length to the distribution (5) increases logarithmically. Consequently, the results of numerical simulations confirm the possibility of adiabatic transition to the $\pm$ mode in the process of wave beam amplification.

VII. COMPARISON WITH DIRECT SIMULATIONS

To verify the stability of the analytic solutions found above in the frame of the single-mode approximation, we performed numerical simulation of the wave field dynamics described by the nonlinear unidirectional wave propagation equation [39],

$$i\frac{\partial \mathcal{E}}{\partial z} = \sqrt{k_0^2 n_0^2 + \Delta_\perp}\,\mathcal{E} + k_0 n_2 |\mathcal{E}|^2 \mathcal{E} + k_0 U(x,y)\mathcal{E}, \tag{33}$$

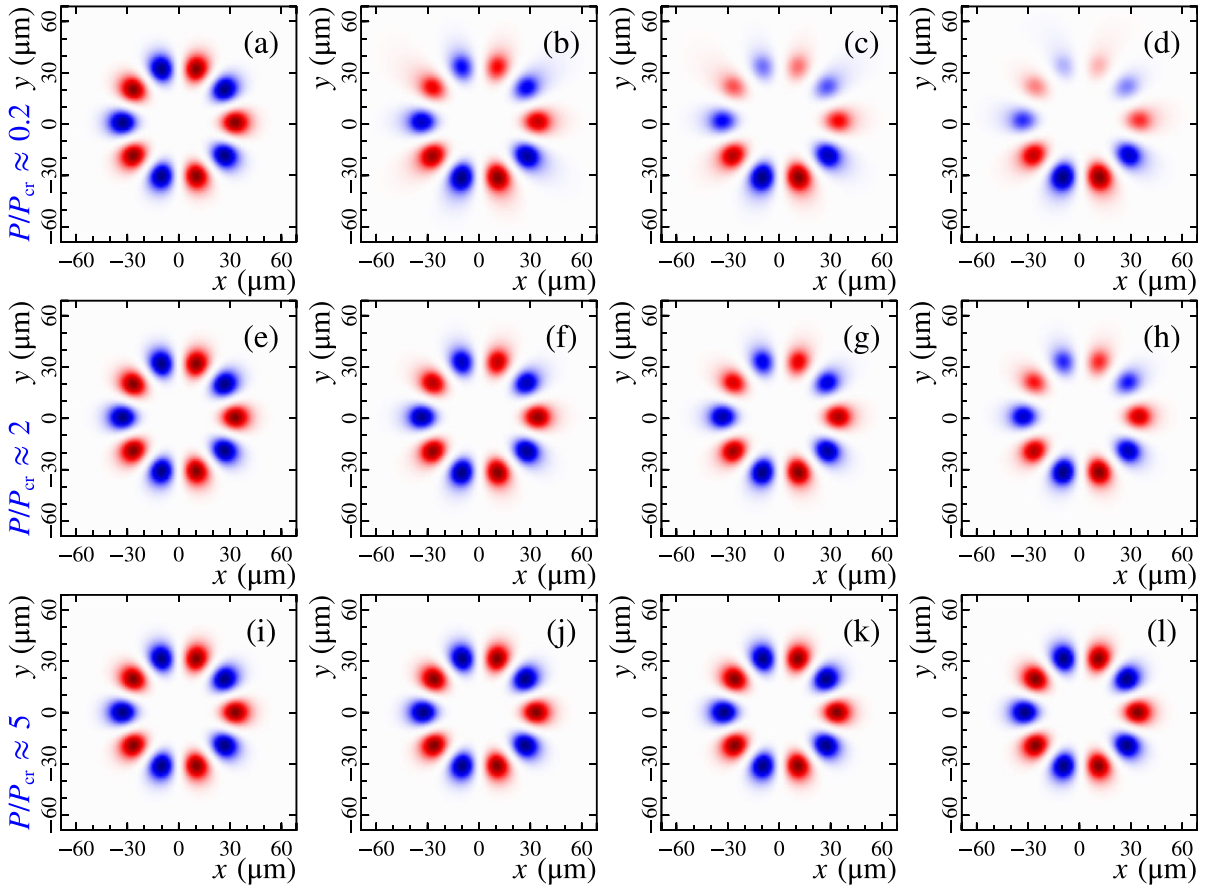

FIG. 6. Distributions of $|u|\mathrm{Re}u$ of the wave fields corresponding to different powers $\mathcal{P}/\mathcal{P}_{cr} = 0.2$ (a)–(d), $\mathcal{P}/\mathcal{P}_{cr} = 2$ (e)–(h), $\mathcal{P}/\mathcal{P}_{cr} = 5$ (i)–(l). The inhomogeneoity lengths are $L = 0$ (a), (e), and (i); $L = 1.5$ mm (b), (f), and (j); $L = 0.75$ mm (c), (g), and (k); $L = 0.5$ mm (d), (h), and (l).

with the potential,

$$U = y/L + \delta n \sum_n \exp\left(-\left[\frac{(x-x_n)^2 + (y-y_n)^2}{r_n^2}\right]^4\right).$$

Here, x_n, y_n, r_n are the position and radius of the cores, n_0 is the refractive index of the cladding, δn is the difference between the refractive indices of the cores and the medium, n_2 is the nonlinear refractive index, and L is the length of media inhomogeneity. The operator $\sqrt{k_0^2 n_0^2 + \Delta_\perp}$ can be easily calculated in Fourier space, and allows one to properly describe wave fields with transverse scales being of the order of the wavelength with spherical aberrations taken into account.

Numerical simulations were carried out at the wavelength $2\pi/k_0 = 1.03\,\mu$m for a silica fiber, similar to that available to our group. The refractive index of the cladding was taken to be $n_0 = 1.45$. The difference in the refractive indices between the cores and the cladding was $\delta n = 0.002$. The nonlinear refractive index was $n_2 = 3\times10^{-16}$ cm^2/W. The radii of the cores were equal to $r_n = 7\,\mu$m, and the distance between them was $20\,\mu$m. The simulation was performed on a grid with the number of points 256×256 in a plane perpendicular to the propagation direction. The calculation step along the fiber axis was chosen to be $\Delta z = 1\,\mu$m. We have confirmed that reducing the step by half (with a corresponding increase in the number of points along any coordinate) does not lead to a change in numerical results.

The initial wave field distributions were chosen as the found analytic solution for u_n multiplied by $\psi(x, y) = 1/\cosh(\sqrt{x^2 + y^2}/7\,\mu\mathrm{m})$. The fields $\psi(x, y)$ in each core are close to the fundamental mode of an individual core. This simplified form of the initial distribution introduces appreciable noise up to the level of 3% of the amplitude of the exact solution. Since the presented solutions are stable, such simplification did not lead to a noticeable distortion of the wave field structure, but gave only small amplitude and phase oscillations.

Direct numerical simulation of Eq. (33) showed good stability of most of the found solutions (Fig. 6). Moreover, direct numerical simulations confirm the conclusion made within the framework of the discrete model that an increase in the total power of the wave beam leads to more uniform distribution of the wave amplitudes across the MCF cores.

VIII. SPATIOTEMPORAL SOLITONS

In the previous sections, stable stationary nonlinear solutions were found, which ensures the coherent propagation of wave beams in strongly deformed MCF. Further interest

here is related to the possibility of coherent propagation of solitonlike laser pulses in strongly bent MCF, i.e., the ability to transmit laser pulses without changing the temporal structure along an extended path.

Equation (3) must be supplemented by the dispersion term to describe the dynamics of the spatiotemporal soliton. In this section, we restrict ourselves to media with $\gamma_n = 0$ and with the simplest form of deformations (7). As a result, we arrive at the equation

$$i\frac{\partial u_n}{\partial z} = \frac{\partial^2 u_n}{\partial \tau^2} + |u_n|^2 u_n + u_{n+1} + u_{n-1} + D\sin\left(\frac{n\pi}{N}\right)u_n, \tag{34}$$

where the longitudinal coordinate τ is normalized by $\sqrt{|k_2|/2\chi}$, $k_2 = \frac{\partial^2 \kappa}{\partial \omega^2}$. Equation (34) conserves total energy,

$$W = \sum_{n=1}^{2N} \int |u_n|^2 d\tau = \text{const}. \tag{35}$$

The exact analytical solution was found for ideal MCF ($D = 0$) in the form of a spatiotemporal soliton [29],

$$u_n = (-1)^n \frac{\sqrt{2}b}{\cosh(b\tau)} e^{i(2-b^2)z}, \tag{36}$$

with out-of-phase distribution in the transverse direction. Its stability is proved both with respect to small perturbations of the wave field, including azimuthal ones, and with respect to small deformations of the MCF structure.

The method developed in Sec. V for finding exact stationary solutions for wave beams in strongly bent MCFs can be generalized to the case of pulsed radiation. Next, we analyze the simplest case of six cores ($N = 3$). A solution can be sought in factorized form, similar to (21)

$$u_n = \sqrt{\frac{W}{6\tau_p}} \frac{e^{i\sigma + i\alpha\tau^2}}{\cosh(\tau/\tau_p)} \left[C\frac{(-1)^n}{\sqrt{2}} + Be^{i\phi}\sin\frac{2\pi n}{3} + Ae^{i\theta}\cos\frac{\pi n}{3} \right], \tag{37}$$

where $C = \sqrt{1 - A^2 - B^2}$, W and τ_p are the total energy (35) and the duration of the spatiotemporal soliton, α is a parameter of the frequency chirp, and ϕ and θ are relative phase differences. Such approximation is applicable if the dispersion length is larger than the coupling one: $\tau_p^2 \gg 1$.

Using the variational approach to the distribution (37) along the coordinate τ, we obtain equations for the parameters of the wave packet. Its stationary solution is located at $\phi = \theta = \alpha = 0$ and the soliton duration,

$$\tau_p = \frac{48/W}{2 - 4\sqrt{2}(3B^2 - A^2)AC - 7(A^2 + B^2)^2 + 8(A^2 + B^2)}. \tag{38}$$

Thus, the dispersion length $\tau_p^2 \propto 1/W^2$ is essentially a nonlinear length for spatiotemporal solitons. The stationary values of the coefficients A and B correspond to the minimum point of the Hamiltonian, similar to (24):

$$H_s = ABD + B^2 + 3A^2 - \sqrt{2}DBC + (3B^2 - A^2)ACW^2\frac{7(A^2 + B^2)^2 - 8(A^2 + B^2) - 2}{6^3 2\sqrt{2}} + [7(A^2 + B^2)^2 - 8(A^2 + B^2) - 2]^2\frac{W^2}{6^3 32} + \frac{W^2}{6^3}(B^2 + A^2 - 1)(3B^2 - A^2)^2. \tag{39}$$

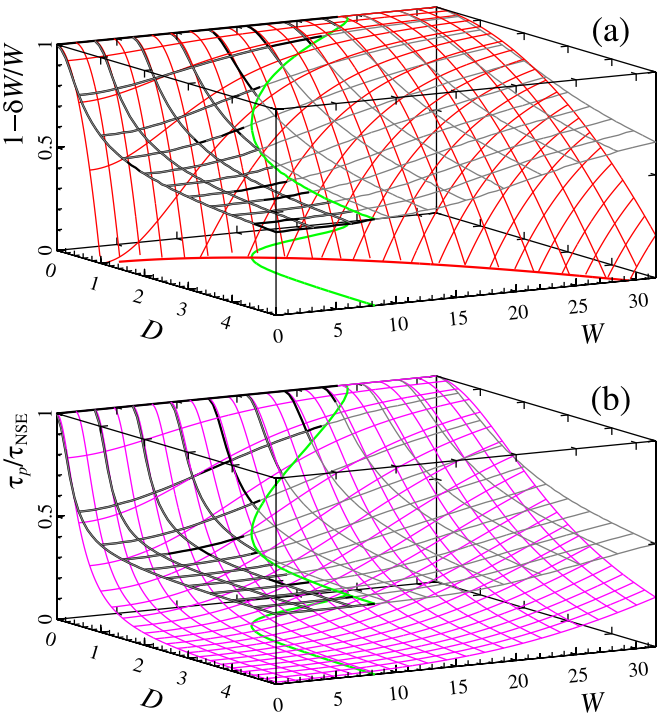

FIG. 7. (a) Dependence of the energy fraction $\eta_\pm$ of the spatiotemporal soliton solution in the $\pm$ mode on the perturbations amplitude D and on the total energy W. Here the black surface is built on the basis of the found minima of Eq. (39); the red (gray) surface corresponds to the estimate (43). (b) The dependence of τ_p/τ_{NSE} on D and W is shown by the black surface; the magenta (gray) surface corresponds to the estimate (42). The green (light gray) curve shows the stability boundary of the solution $\tau_p = 1$.

The most uniform energy distribution over MCF cores corresponds to the out-of-phase mode, for which the value $A^2 + B^2$ is closest to 0. The asymptotic behavior of this solution at high energies W has the form,

$$B_\pm \approx \frac{1}{\sqrt{2}}\frac{D}{1 + W^2/6^3} + O(D^3/W^6), \tag{40}$$

$$A_\pm \approx \frac{1}{4\sqrt{2}}\frac{D^2}{\left(\frac{7}{2} + W^2/6^3\right)^2} + O(D^4/W^8). \tag{41}$$

The knowledge of these asymptotics allows one to find expressions of the spatiotemporal soliton duration τ_p and the fraction of energy $\eta_\pm = 1 - \delta W/W$ in the $\pm$ mode,

$$\frac{\tau_p}{\tau_{\text{NSE}}} \approx \frac{1}{1 + 4B_\pm^2} \approx \frac{(1 + W^2/6^3)^2}{(1 + W^2/6^3)^2 + 2D^2}, \tag{42}$$

$$\eta_\pm = 1 - \frac{\delta W}{W} = C^2 \approx 1 - \frac{D^2/2}{(1 + W^2/6^3)^2}. \tag{43}$$

Here $\tau_{\text{NSE}} = 4/W_{\text{NSE}}$ is the duration of the NSE soliton in the case of uniform distribution of energy over the cores: $W_{\text{NSE}} = W/6$.

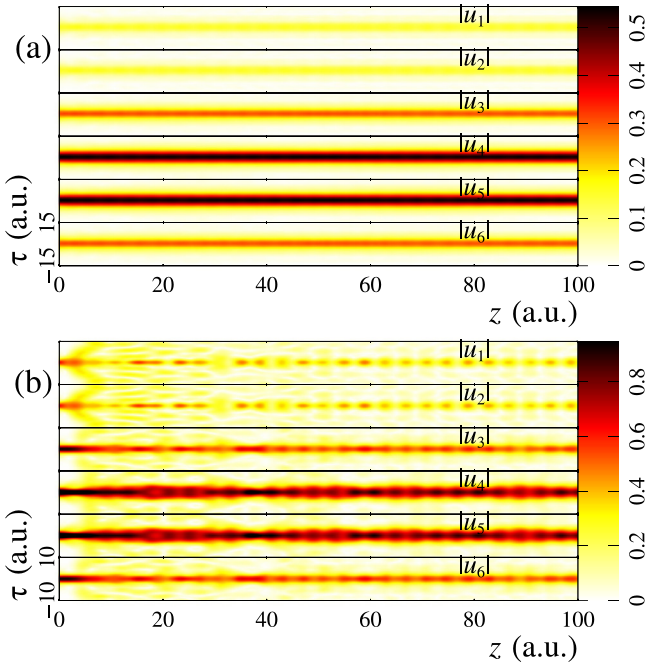

FIG. 8. The evolution of the wave packet amplitude in a deformed six-core MCF with $D = 1$. The initial distribution of the wave packet corresponds to the found solution (37) for different values of the total energy W: (a) $W = 5$ with the dispersion length equal to 8; (b) $W = 15$ with the dispersion length equal to 1.

Let us compare the exact solution and the found asymptotics (42) and (43). In Fig. 7(a), the black surface shows the dependence of the fraction of energy $\eta_{\pm}$ of the found solution on the total energy W and on the amplitude of the perturbations D. The red (gray) surface corresponds to the asymptotic (43). This figure shows that the fraction of energy in the $\pm$ mode tends to unity with increasing total energy W of the wave packet. In Fig. 7(b), the black surface shows the dependence of $\tau_p/\tau_{\mathrm{NSE}}$ on D and W, and the magenta (gray) one shows the asymptotic (42). This figure shows that the duration τ_p of the found solution tends to the duration τ_{NSE} of the NSE soliton with an increase in the total energy W. The green curve in Fig. 7 shows the applicability boundary $\tau_p = 1$. Found approximations are in good agreement with exact solutions for deformation amplitudes $D \leqslant 1 + W^2/6^3$.

We check the stability of obtained approximate solutions in the framework of the numerical simulation of Eq. (34). Figure 8 shows the evolution of the wave packet in a deformed MCF of six cores in the case $D = 1$. The initial distribution of the wave packet corresponds to the found solution (37) for different values of the total energy W. For a small energy $W = 5$, the dispersion length exceeds the coupling length, which is a necessary condition for the existence of the found solution. The results of numerical simulations confirm the stability of the found solution [Fig. 8(a)]. The fraction of energy in the $\eta_{\pm}$ mode is 77%. The case of the total energy $W = 15$ is on the boundary of the solution applicability, since the dispersion length becomes approximately equal to the coupling length. Nevertheless, the wave structure as a whole isn't destroyed [Fig. 8(b)], but beats are observed. The fraction of energy in the $\pm$ mode is about 90%. A further increase in energy leads to stronger beats that destroy the wave packet structure both in the longitudinal and transverse directions.

Thus, a substantial equalizing of the energy distribution over MCF cores cannot be achieved, since it is limited to the region of existence of the solutions $\tau_p^2 \geqslant 1$. In dimensional units, this condition corresponds to pulses with durations longer than $\sqrt{|k_2|/(2\chi)}$. For the typical coupling coefficients $\chi \approx 0.1 \ldots 1\,\mathrm{cm}^{-1}$ and the dispersion $k_2 \approx -15\,\mathrm{ps}^2/\mathrm{km}$, the limiting durations are 9...27 fs and lie obviously outside the range of applicability of the original equation (34).

IX. CONCLUSION

In this paper, we examined the propagation of laser pulses in MCF consisting of an even number $2N$ of cores located around a ring. Main attention was paid to the transformation of the out-of-phase wave field distribution during structure deformations of the multicore fiber, including fiber bending and gain inhomogeneity in different cores.

In the case of small deformations leading to a small perturbation of the propagation constant in comparison with the coupling coefficient, approximate solutions are obtained. Moreover, the power fraction in the perturbations is a quantity of the next order of smallness in the deformation amplitude. The reason is the orthogonality of the $\pm$ mode $u_n \propto (-1)^n$ to all other fiber eigenmodes. A similar conclusion can be made for the active fiber, including ones with a small gain inhomogeneity. The analytical analysis is confirmed by the results of numerical simulations.

An increase in the deformation amplitude leads to an increasing deviation of the out-of-phase distribution from the ideal case of the $\pm$ mode. A complete analysis of resulting equations is difficult. The situation is greatly simplified when searching for stationary solutions in the case of odd N: It is enough to solve the system of $N - 1$ nonlinear algebraic equations for the amplitudes of linear eigenmodes, and then check the stability of the resulting solution. Thus, the task, although technically difficult, becomes quite accessible for modern computer algebra systems (Fig. 4). As an example, the simplest case $N = 3$, when the stationary solution is determined by only two real coefficients, is considered in detail.

An analysis of the obtained solutions showed that the nonuniformity of the wave field amplitude in different cores decreases with an increase in the total radiation power. This means that the total transported power can be $2N$ times higher than the critical self-focusing power in a homogeneous medium even in a strongly deformed MCF. In particular, wave beam amplification, which has the form of the found out-of-phase solution in an active MCF even with a strong difference in the refractive indices in the cores, leads to equalization of the wave field amplitudes at powers larger than the found critical value. This result is confirmed by direct numerical simulations (Fig. 6).

A generalization of this technique to the case of wave packets allowed us to find a stable approximate stationary solution in the form of spatiotemporal solitons. Their existence and stability is confirmed by direct numerical simulation.

Unfortunately, the condition for the stability of found solutions (a smallness of coupling bond length in comparison with the dispersion one) makes it impossible to substantially equalize the energy distribution over MCF cores.

ACKNOWLEDGMENT

This work was supported by the Russian Science Foundation (Grant No. 16-12-10472).

[1] G. Mourou, T. Tajima, M. N. Quinn, B. Brocklesby, and J. Limpert, Nucl. Instrum. Methods Phys. Res. A **740**, 17 (2014).
[2] G. Mourou, B. Brocklesby, T. Tajima, and J. Limpert, Nat. Photon. **7**, 258 (2013).
[3] M. Müller, M. Kienel, A. Klenke, Th. Gottschall, E. Shestaev, M. Plötner, J. Limpert, and A. Tünnermann, Opt. Lett. **41**, 3439 (2016).
[4] J. Bourderionnet, C. Bellanger, J. Primot, and A. Brignon, Opt. Exp. **19**, 17053 (2011).
[5] A. Klenke, M. Müller, H. Stark, M. Kienel, C. Jauregui, A. Tünnermann, and J. Limpert, IEEE J. Sel. Top. Quantum Electron. **24**, 0902709 (2018).
[6] A. Scott, *Nonlinear Science. Emergence and Dynamics of Coherent Structures* (Oxford University Press, Oxford, 2003).
[7] D. N. Christodoulides, F. Lederer, and Y. Silberberg, Nature (London) **424**, 817 (2003).
[8] Y. Kivshar and G. Agrawal, *Optical Solitons. From Fibers to Photonic Crystals* (Academic Press, Cambridge, 2005).
[9] A. B. Aceves, C. De Angelis, S. Trillo, and S. Wabnitz, Opt. Lett. **19**, 332 (1994).
[10] A. B. Aceves, C. De Angelis, T. Peschel, R. Muschall, F. Lederer, S. Trillo, and S. Wabnitz, Phys. Rev. E **53**, 1172 (1996).
[11] D. N. Christodoulides and R. I. Joseph, Opt. Lett. **13**, 794 (1988).
[12] H. S. Eisenberg, Y. Silberberg, R. Morandotti, A. R. Boyd, and J. S. Aitchison, Phys. Rev. Lett. **81**, 3383 (1998).
[13] A. B. Aceves, A. M. Rubenchik, S. K. Turitsyn, and C. De Angelis, Opt. Lett. **19**, 329 (1994).
[14] E. W. Laedke, K. H. Spatschek, and S. K. Turitsyn, Phys. Rev. Lett. **73**, 1055 (1994).
[15] H. Leblond, D. Kremer, and D. Mihalache, Phys. Rev. A **95**, 043839 (2017).
[16] D. Mihalache, D. Mazilu, F. Lederer, Y. V. Kartashov, L. C. Crasovan, and L. Torner, Phys. Rev. E **70**, 055603(R) (2004).
[17] N. K. Efremidis and D. N. Christodoulides, Phys. Rev. E **67**, 026606 (2003).
[18] N. K. Efremidis, D. N. Christodoulides, and K. Hizanidis, Phys. Rev. A **76**, 043839 (2007).
[19] J. M. Soto-Crespo, N. Akhmediev, and A. Ankiewicz, Phys. Lett. A **314**, 126 (2003).
[20] D. Mihalache, D. Mazilu, and F. Lederer, Eur. Phys. J. Spec. Top. **173**, 255 (2009).
[21] A. A. Balakin, A. G. Litvak, V. A. Mironov, and S. A. Skobelev, Phys. Rev. A **94**, 063806 (2016).
[22] A. A. Balakin, A. G. Litvak, V. A. Mironov, and S. A. Skobelev, Laser Phys. **28**, 045401 (2018).
[23] A. B. Aceves, G. G. Luther, C. De Angelis, A. M. Rubenchik, and S. K. Turitsyn, Phys. Rev. Lett. **75**, 73 (1995).
[24] I. S. Chekhovskoy, A. M. Rubenchik, O. V. Shtyrina, M. P. Fedoruk, and S. K. Turitsyn, Phys. Rev. A **94**, 043848 (2016).
[25] A. M. Rubenchik, I. S. Chekhovskoy, M. P. Fedoruk, O. V. Shtyrina, and S. K. Turitsyn, Opt. Lett. **40**, 721 (2015).
[26] A. V. Andrianov, N. A. Kalinin, M. Y. Koptev, O. N. Egorova, A. V. Kim, and A. G. Litvak, Opt. Lett. **44**, 303 (2019).
[27] D. Cheskis, S. Bar-Ad, R. Morandotti, J. S. Aitchison, H. S. Eisenberg, Y. Silberberg, and D. Ross, Phys. Rev. Lett. **91**, 223901 (2003).
[28] H. S. Eisenberg, R. Morandotti, Y. Silberberg, S. Bar-Ad, D. Ross, and J. S. Aitchison, Phys. Rev. Lett. **87**, 043902 (2001).
[29] A. A. Balakin, A. G. Litvak, and S. A. Skobelev, Phys. Rev. A **100**, 053834 (2019).
[30] T. X. Tran, D. C. Duong, and F. Biancalana, Phys. Rev. A **90**, 023857 (2014).
[31] A. A. Balakin, A. G. Litvak, and S. A. Skobelev, Phys. Rev. A **100**, 053830 (2019).
[32] A. A. Balakin, S. A. Skobelev, A. V. Andrianov, N. A. Kalinin, and A. G. Litvak, Opt. Lett. **44**, 5085 (2019).
[33] A. B. Aceves, O. V. Shtyrina, A. M. Rubenchik, M. P. Fedoruk, and S. K. Turitsyn, Phys. Rev. A **91**, 033810 (2015).
[34] S. Minardi, F. Eilenberger, Y. V. Kartashov, A. Szameit, U. Ropke, J. Kobelke, K. Schuster, H. Bartelt, S. Nolte, L. Torner, F. Lederer, A. Tunnermann, and T. Pertsch, Phys. Rev. Lett. **105**, 263901 (2010).
[35] F. Eilenberger, S. Minardi, A. Szameit, U. Ropke, J. Kobelke, K. Schuster, H. Bartelt, S. Nolte, L. Torner, F. Lederer, A. Tunnermann, and T. Pertsch, Phys. Rev. A **84**, 013836 (2011).
[36] V. E. Lobanov, Y. V. Kartashov, and L. Torner, Phys. Rev. Lett. **105**, 033901 (2010).
[37] S. K. Turitsyn, A. M. Rubenchik, M. P. Fedoruk, and E. Tkachenko, Phys. Rev. A **86**, 031804(R) (2012).
[38] A. M. Rubenchik, E. V. Tkachenko, M. P. Fedoruk, and S. K. Turitsyn, Opt. Lett. **38**, 4232 (2013).
[39] A. A. Balakin, S. A. Skobelev, E. A. Anashkina, A. V. Andrianov, and A. G. Litvak, Phys. Rev. A **98**, 043857 (2018).